Mean and Turbulent Flow Downstream of a Low-Intensity Fire: Influence of Canopy and Background Atmospheric Conditions

MICHAEL T. KIEFER

Department of Geography, Michigan State University, East Lansing, Michigan

WARREN E. HEILMAN

Northern Research Station, U.S. Department of Agriculture Forest Service, Lansing, Michigan

SHIYUAN ZHONG

Department of Geography, Michigan State University, East Lansing, Michigan

JOSEPH J. CHARNEY AND XINDI BIAN

Northern Research Station, U.S. Department of Agriculture Forest Service, Lansing, Michigan

(Manuscript received 25 February 2014, in final form 25 September 2014)

ABSTRACT

This study examines the sensitivity of mean and turbulent flow in the planetary boundary layer and roughness sublayer to a low-intensity fire and evaluates whether the sensitivity is dependent on canopy and background atmospheric properties. The ARPS-CANOPY model, a modified version of the Advanced Regional Prediction System (ARPS) model with a canopy parameterization, is utilized for this purpose. A series of numerical experiments are conducted to evaluate whether the ability of the fire to alter downstream wind, temperature, turbulent kinetic energy (TKE), and vertical heat flux differs between forested and open areas, sparse and dense forests, weak and strong background flow, and neutral and convective background stability. Analysis of all experiments shows that, in general, mean and turbulent flow both prior to and during a low-intensity fire is damped in the presence of a canopy. Greater sensitivity to the fire is found in cases with strong ambient wind speed than in cases with quiescent or weak wind speed. Furthermore, sensitivity of downstream atmospheric conditions to the fire is shown to be strongest with a neutrally stratified background. An analysis of the TKE budget reveals that both buoyancy and wind shear contribute to TKE production during the period of time in which the fire conditions are applied to the model. On the basis of the results of the ARPS simulations, caution is advised when applying ARPS-simulation results to predictions of smoke transport and dispersion: smoke-model users should consider whether canopy impacts on the atmosphere are accounted for and whether neutral stratification is assumed.

1. Introduction

The role of the heat output from a wildland fire in perturbing the atmosphere has been examined to varying degrees with numerical models for approximately 20 years. To date, examination of the atmospheric response to the heat output from wildland fires by the fire weather research community has largely focused on higher-intensity fires [mean parameterized vertical heat fluxes $O(15–100+\ \mathrm{kW\,m^{-2}})$] (e.g., Heilman and Fast 1992; Cunningham et al. 2005; R. Sun et al. 2006, 2009; Kiefer et al. 2009). Examples of fire-induced atmospheric phenomena that have been studied with numerical models include vortices (e.g., Heilman and Fast 1992; Cunningham et al. 2005), storm–mesoscale dry convection (e.g., Kiefer et al. 2008, 2009), and planetary boundary layer (PBL) turbulence (e.g., Sun et al. 2009). The studied phenomena span a range of spatial scales, from as small as the scale of individual flames (10^{-3}–10^{0} m) to as large as mesoscale (2×10^{3}–2×10^{6} m), and may impact fire behavior as well as smoke transport and dispersion.

Corresponding author address: Michael Kiefer, Michigan State University, Geography Bldg., 673 Auditorium Rd. Rm. 203, East Lansing, MI 48824.
E-mail: mtkiefer@msu.edu

DOI: 10.1175/JAMC-D-14-0058.1

In general, the effect of a vegetation canopy on the atmospheric response has been ignored, with several notable exceptions. For example, Cunningham et al. (2005) accounted for the effect of a forest canopy on wind by adding a drag term to the momentum equation in the Weather Research and Forecasting (WRF) Model (Skamarock et al. 2005); the drag term was applied only at the grid point closest to the ground surface, however. In addition, Pimont et al. (2011) used the "FIRETEC" model (Linn and Cunningham 2005; Pimont et al. 2009) to examine the sensitivity of wind flow and fire propagation to structural parameters of a multiple grid-level forest canopy, including tree-cover fraction and clump size.

How fires—in particular, low-intensity fires—perturb the atmosphere in and above a forest canopy within several kilometers of the fire has received little examination and attention. Fire-induced changes to the ambient flow are potentially relevant to smoke behavior since transport and dispersion of smoke from wildland fires may be sensitive to the local mean and turbulent flow in and above vegetation canopies (e.g., Heilman et al. 2013). In this study, we use a numerical model to examine atmospheric sensitivity to a low-intensity fire within a forested region. Research into how low-intensity fires beneath forest canopies perturb the local environment has particular relevance for prediction of smoke transport and dispersion during prescribed fire events since prescribed fires, as compared with wildfires, are more likely to be of lower intensity. Prescribed fire is one of the tools used by land managers to achieve land-management goals in agricultural and forested environments, with 20.2 million acres in the United States treated in 2011 alone (Melvin 2012). These managed fires may produce peak heat fluxes that are comparable in magnitude to those of wildfires, but the smaller scale of the fires and the shorter duration of heating generally limit the overall quantity of heat output (Heilman et al. 2013).

In this study, we examine whether the sensitivity of mean and turbulent flow in the PBL and roughness sublayer (~2–5 times canopy height) to a low-intensity fire ($5\,\mathrm{kW\,m^{-2}}$ of surface heat flux) is dependent on canopy and background atmospheric properties. In other words, we seek to understand whether the ability of the fire to alter downstream wind, temperature, turbulent kinetic energy (TKE), and vertical heat flux differs between forested and open areas, sparse and dense forests, weak and strong background flow, and neutral and convective background stability. Owing to computational restraints, we do not endeavor to explicitly resolve small-scale [$O(10\,\mathrm{m})$] thermal plumes in the immediate vicinity of the fire but instead opt to parameterize such small-scale turbulent structures (see section 2) and to focus on a broad region downstream of the fire. In addition to the examination of atmospheric flow sensitivity, we also wish to evaluate the underlying dynamics behind the atmospheric response within several kilometers of a low-intensity fire. Thus, we examine TKE budgets both prior to and during the fire to understand better how production, transport, and dissipation of turbulence are altered as a result of the presence of a low-intensity fire.

To achieve these stated goals we use the ARPS-CANOPY canopy-flow model (Kiefer et al. 2013), which is a modified version of the Advanced Regional Prediction System (ARPS) model (Xue et al. 2000, 2001) in which the effects of vegetation elements (e.g., branches or leaves) on drag, turbulence production/dissipation, radiation transfer, and the surface energy budget are accounted for through modifications to the ARPS model equations. As stated in Kiefer et al. (2013), although ARPS and ARPS-CANOPY can be run in either Reynolds-averaged Navier–Stokes mode [at scales $O(1\,\mathrm{km})$ or larger] or large-eddy simulation (LES) mode [at scales $O(10\,\mathrm{m})$ or smaller], the need to apply the model in near-real-time mode for potential operational smoke-dispersion prediction efforts demands that a hybrid approach be used. Thus, in this study, we apply ARPS-CANOPY with grid dimensions that neither preclude the explicit resolution of turbulent motions nor guarantee that the bulk of TKE is contained within the resolved turbulent motions (i.e., not true LES) [for other examples of this approach, see H. Sun et al. (2006), Michioka and Chow (2008), and Kiefer et al. (2014)].

The remainder of this paper is organized as follows. A description of the model and experiment design is presented, including a brief overview of the ARPS-CANOPY model and how it differs from the standard ARPS model (section 2a), a description of the model configuration and parameterization (section 2b), and a summary of the experiment design (section 2c). Results from the sensitivity experiments are then presented , including an overview of all 14 cases (section 3a), an examination of scalar fluxes in the PBL in a subset of cases (section 3b), and an analysis of the budget of grid-resolved TKE in a smaller subset of cases (section 3c). The paper is concluded in section 4.

2. Model description and numerical design

a. *ARPS-CANOPY overview*

ARPS is a fully compressible, nonhydrostatic atmospheric modeling system with terrain-following coordinates. ARPS is a flexible model that may be applied with grid spacing as fine as $O(1\,\mathrm{m})$ for studies of turbulent flows (e.g., Dupont and Brunet 2008, 2009) or with much coarser grid spacing of $O(1\text{–}10\,\mathrm{km})$ for studies of mesoscale and synoptic-scale phenomena

(e.g., Xue et al. 2003; Parker and Johnson 2004; Michioka and Chow 2008). A modified version of ARPS was developed by Kiefer et al. (2013), on the basis of earlier modifications made by Dupont and Brunet (2008), to account for the effects of vegetation elements on flow through a vegetation canopy. ARPS-CANOPY has been applied to flows through a homogeneous orchard canopy (Kiefer et al. 2013) and a heterogeneous forest canopy (Kiefer et al. 2014) as well as to flows along the sidewalls of an idealized valley (Kiefer and Zhong 2013).

A brief overview of ARPS-CANOPY follows; for more details, see Kiefer et al. (2013). ARPS-CANOPY is an expansion of a version of ARPS that was developed by Dupont and Brunet (2008) to allow for simulation of flow inside and above a forest canopy. In the model developed by Dupont and Brunet (2008), terms were added to the ARPS momentum and subgrid-scale (SGS) TKE equations to account for drag associated with canopy elements and enhancement of turbulence dissipation in the canopy air space, respectively. Kiefer et al. (2013) subsequently added a production term to the SGS TKE equation to account for the generation of SGS TKE in the wakes of canopy elements, following work by Kanda and Hino (1994). Additional modifications to ARPS made by Kiefer et al. (2013) were designed to allow ARPS to explicitly simulate nonneutrally stratified flows inside and above forest canopies. Following an approach outlined in H. Sun et al. (2006), a series of equations was added to the ARPS radiation physics module first to compute net radiation at canopy top and second to prescribe a net radiation profile inside the canopy with a profile shape that approximates an exponential decay of net radiation with descending height in a canopy. In addition, the ARPS thermodynamic equation was expanded to include a term representing the heating (cooling) of the atmosphere inside the canopy resulting from the vertical flux convergence (divergence) of net radiation intercepted by the canopy. Last, the ARPS module that computes ground net radiation was modified to account for the shading of the ground surface during the day and reduction of outgoing longwave radiation beneath the canopy at night.

Note that ARPS-CANOPY does not resolve the flow around individual trees or calculate the heating/cooling of individual canopy elements (e.g., leaves). In all aspects of the canopy parameterization, the canopy is represented by a height-varying profile of plant-area density A_p, defined as the one-sided area of all plant material per unit volume of the canopy. Parameter A_p is a measure of the density of vegetation elements averaged across a group of trees [$O(50)$ trees for the grid spacing used in this study] and is specified at each grid point.

b. Model configuration and parameterization

With the exception of the modifications outlined in the prior section, ARPS-CANOPY is identical to standard ARPS. A 1.5-order subgrid-scale turbulence closure scheme with a prognostic equation for TKE is utilized, and radiation physics following Chou (1990, 1992) and Chou and Suarez (1994) are applied outside of the canopy. Fourth-order-accurate finite differencing of the advection terms is used in both the vertical and horizontal directions. The Coriolis force is computed (as a function of central latitude only), and moist processes are omitted in all simulations.

A three-dimensional computational domain is utilized, with the domain extending 10 km in the x direction, 7.5 km in the y direction, and 3 km in the z direction. Horizontal grid spacing is 50 m, and vertical grid spacing is 2 m up to a height of 84 m, above which vertical stretching is applied. A periodic boundary condition is applied at all lateral boundaries, and the upper boundary condition is a sponge layer extending from height z = 2 km to the model top. For all simulations, ARPS has horizontally homogeneous initial conditions. A base-state sounding is used to initialize each simulation, consisting of uniform wind speed from the surface to domain top and neutral static stability below z = 1 km (stable stratification above). The model is initialized at noon local time, with a uniform net radiation flux of 520 W m^{-2} applied at the canopy top (or ground surface in simulations without a canopy) to represent daytime heating typical of 40°N in early spring. An exception to the homogeneity is that a random perturbation (of magnitude 1 K) is applied to the potential temperature field at the initial time (at all model levels) to promote the development of 3D turbulent structures.

c. Experiment design

The model is run for 3 h to ensure the development of a horizontally quasi-homogeneous and quasi-stationary PBL before a 5 kW m^{-2} surface turbulent sensible heat flux, representative of a low-intensity fire, is applied along a north–south-oriented strip that is positioned 3.15 km downstream of the western boundary. The heat-source strip is one grid point wide and, as a consequence of the periodic lateral boundary condition, is assumed to be infinitely long. The reader should keep the infinite fire length in mind when interpreting results from this study, because air is unable to flow around the fire and three-dimensional phenomena such as line-end vortices are not simulated.

Real fire lines are seldom as wide as 50 m, and therefore a simulation employing 50-m grid spacing is not capable of fully resolving the heat flux from a narrower,

more intense fire line. Datasets of in situ meteorological measurements within actively burning zones are limited in number (e.g., Clements et al. 2007), mainly because of the damaging effects of high temperatures on instrumentation and the inherent danger to personnel. Nonetheless, in situ measurements have been obtained during a number of low-intensity prescribed fires, with peak 1-min mean vertical turbulent heat fluxes measured during recent fires in the New Jersey Pine Barrens (Heilman et al. 2013) ranging between 8 and 155 kW m^{-2} and values reported during other experiments [e.g., FireFlux 1 from Clements et al. (2007) and the Prescribed Fire Combustion and Atmospheric Dynamics Research Experiment (RxCADRE) in Hiers et al. (2009)] falling within this envelope. These heat fluxes were observed at a single point in space and persisted for at most 4–5 min. The approach we take in this study is to assume that the heat from a relatively narrow fire line [O(5 m) in width] is distributed across each 50 m × 50 m grid cell; thus, this unresolved fire line if overlaid on the grid cell would constitute no more than 10% of the area of the cell at any given time. Therefore, a 5 kW m^{-2} heat flux applied across a 50 m × 50 m grid cell is consistent with a 50 kW m^{-2} heat flux distributed across a 5-m-wide fire line. This approach is identical to that of Kiefer et al. (2014) and was shown therein to yield profiles of mean wind, temperature, and TKE that agreed favorably with observations made during a low-intensity prescribed burn.

Two series of numerical experiments are conducted, one in which plant-area index

$$P = \int_0^h A_p(z)\, dz$$

is varied (P = 0, 2, 4, 6, and 8) while initial-state (i.e., background) wind speed U is held constant (U = 5 m s^{-1}), and another in which U is varied (U = 0, 5, and 10 m s^{-1}) while P is held constant (P = 2). At all points in the domain, A_p is specified as in Fig. 1, with P varied between experiments by multiplying the A_p values in Fig. 1 by an appropriate factor; in all cases, the height h of the canopy is 18 m. In all simulations, the v component of the wind is set to zero at initialization (i.e., U is oriented normal to the fire line). Each experiment is performed twice, once with the aforementioned 520 W m^{-2} ambient net radiation flux applied (denoted as convective background, or C) and an additional time with the ambient radiation flux omitted (denoted as neutral background, or N). Here and throughout this paper, a naming convention is utilized wherein, for example, U5P2N is a simulation with U = 5 m s^{-1}, P = 2, and no ambient radiation flux (i.e., neutral background). See Table 1 for a summary of experiments.

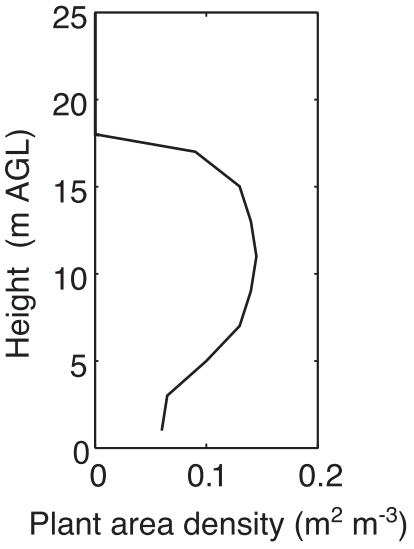

FIG. 1. Example of an A_p profile used in simulations with a forest canopy, for a case with P = 2. For experiments with P = 0, 4, 6, and 8, the displayed A_p profile is multiplied by an appropriate factor.

For each simulation, mean and turbulent variables (e.g., horizontal wind speed or TKE) during the 20-min period after the heat source is switched on (the "fire" period) are compared with corresponding variables from the preceding 20-min period (the "prefire" period). Perturbation wind components u', v', and w' and temperature T' throughout the 40-min period are computed by subtracting the prefire period 20-min mean quantities from the instantaneous values. Use of the prefire mean ensures that modification of the mean variables by the fire does not influence the calculation of perturbations. Instantaneous TKE is subsequently computed as $0.5(u'^2 + v'^2 + w'^2)$, and vertical turbulent heat flux is computed as $w'T'$. Unless otherwise specified, quantities are also averaged spatially over an area downstream of the fire from x = 3.25 km to x = 6.25 km, spanning the entire y dimension.

3. Results and discussion

a. Overview of experiments

We begin with an overview of the sensitivity of downstream mean and turbulent flow to the fire, beginning with an assessment of fire impacts in the roughness sublayer. In Fig. 2, time series of the spatially averaged u component of wind, total TKE (grid resolved + SGS), and temperature are presented for the P experiment series at two levels below canopy top (z/h = 0.06 and z/h = 0.5; left and center panels) and one level above canopy top (z/h = 1.5; right panels). In examining Fig. 2, we find that fire-induced perturbations in the roughness sublayer

TABLE 1. Summary of experiments, wherein U is background wind speed ($m\,s^{-1}$), P is plant-area index, and stability refers to the background state.

Expt	U	P	Stability
U5P0N	5	0	Neutral
U5P0C	5	0	Convective
U5P2N	5	2	Neutral
U5P2C	5	2	Convective
U5P4N	5	4	Neutral
U5P4C	5	4	Convective
U5P6N	5	6	Neutral
U5P6C	5	6	Convective
U5P8N	5	8	Neutral
U5P8C	5	8	Convective
U10P2N	10	2	Neutral
U10P2C	10	2	Convective
U0P2N	0	2	Neutral
U0P2C	0	2	Convective

downwind of the burn zone are largest in the U5P0N (no canopy) case, with perturbations damped in the presence of the forest canopy. In general, cases with a neutral background (e.g., U5P2N) exhibit larger perturbations than cases with a convective background (e.g., U5P2C). An increase in the above-canopy u component of velocity (hereinafter, the fire-line-normal wind component) is evident in the cases with a neutral background, but such a change is nonexistent in the cases with a convective background (Fig. 2c). In fact, variation of fire-line-normal wind velocity and TKE in cases with a convective background is at least as large during the prefire period as during the fire period. Fluctuations in TKE during the prefire period of up to $1\,m^2\,s^{-2}$ are evident at $z/h = 1.5$ in each of the cases with a convective background (Fig. 2f), either occurring entirely in the prefire period (U5P0C and U5P2C) or first appearing in the prefire period and then persisting into the fire period (U5P4C, U5P6C, and U5P8C). The rate of increase of TKE during the fire period is consistent among all cases, regardless of background instability. The increase in spatially averaged temperature downwind of the burn zone is generally less than 1°C, with the magnitude of the increase decreasing with height; the largest fire-induced temperature changes occur in the U5P0N case (Figs. 2g–i).

With regard to the U experiment series (Fig. 3), greater fire-induced changes are again seen in cases with a neutral background, with variability in TKE above the canopy evident during the prefire period in cases with a convective background (Fig. 3f). Changes to the fire-line-normal wind component and TKE are larger in the case with strong ambient wind speed (U10P2N) than in the cases with quiescent or weak ambient wind speeds (U0P2N and U5P2N). Of note is the development of a weak easterly flow in the U0P2 cases, evident at all three levels (see black lines in Figs. 3a–c). Inflow into the convection column above the heat source (not shown) is evident in the absence of prevailing westerly flow but is overwhelmed by the background westerly flow in all other cases.

The spatial averaging procedure used to produce the time series in Figs. 2 and 3 and restriction of the analysis to the roughness sublayer may obscure some of the fire-induced atmospheric perturbations. Analysis of variances at multiple levels inside the PBL [in this study: z = 0–1 km above ground level (AGL)] can help to reveal the impact of the fire on the atmosphere in each of the cases. We choose to limit the analysis to two variables that are closely associated with the vertical movement of smoke: perturbation temperature and vertical velocity. Thus, horizontal profiles of temperature variance ($\langle\overline{T'^2}\rangle$) and vertical velocity variance ($\langle\overline{w'^2}\rangle$) downstream of the fire, averaged temporally over the fire period and spatially across the y domain, are presented in Figs. 4 (P experiment series) and 5 (U experiment series).

Examining the P experiment series first (Fig. 4), we find $\langle\overline{T'^2}\rangle$ as high as $70\,K^2$ at the downstream edge of the fire line, with the magnitude rapidly decreasing with distance downstream of the fire (Fig. 4a). It is notable that the largest $\langle\overline{T'^2}\rangle$ occurs in cases with a neutral background and with a canopy (see inset panel in Fig. 4a). The impact of the fire on downstream temperature is greatest in these cases because of a combination of longer residence times above the fire (light wind speeds inside canopy), relatively weak mixing in the neutrally stratified environment, and an even weaker turbulence environment inside the canopy (Figs. 2d–f). The same quantity of surface heat flux is applied in this study whether a canopy is present or not; with weaker turbulence above the heat source resulting from the presence of the canopy, less mixing occurs and larger temperature perturbations can develop. In the absence of a forest canopy, however, stronger near-surface winds result in shorter residence times and smaller perturbation magnitudes and also serve to advect the higher perturbations downstream, producing a more gradual reduction in $\langle\overline{T'^2}\rangle$ with distance from the fire.

Comparing $\langle\overline{T'^2}\rangle$ and $\langle\overline{w'^2}\rangle$ at multiple levels inside the PBL, we find a corridor of hot rising air emanating from the fire, with variances weakening with height and distance downstream. In contrast to the horizontal profiles inside the canopy, variances at 100 and 500 m AGL are larger in cases with a convective background (Figs. 4c–f). Such behavior is evidence of the prefire atmosphere: perturbations are larger with a convective background than with a neutral background; fire-induced perturbations are superimposed on this prefire state.

Analyzing the U experiment series second (Fig. 5), we find a pattern of $\langle\overline{T'^2}\rangle$ and $\langle\overline{w'^2}\rangle$ downstream of the fire

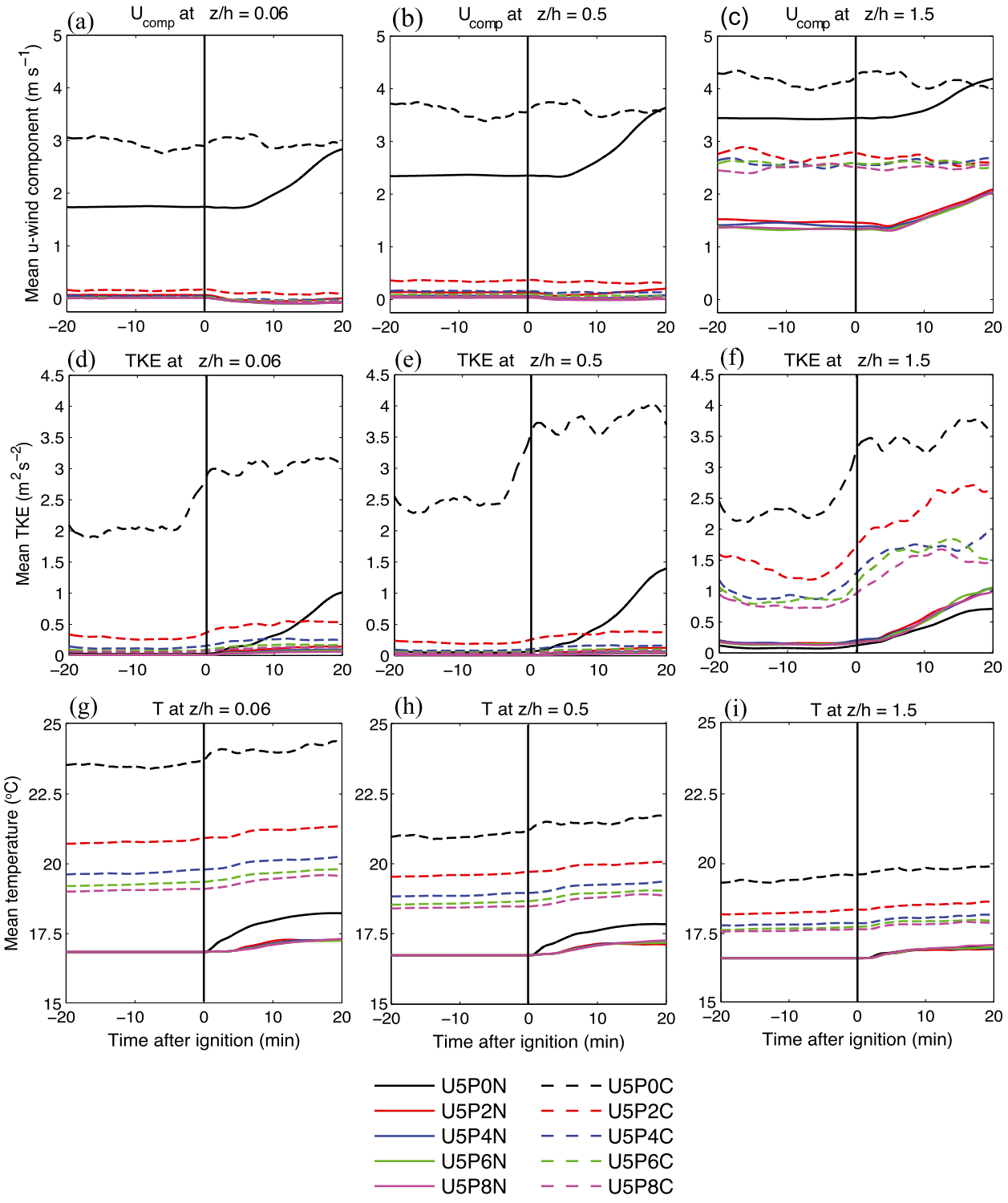

FIG. 2. Time series of spatial mean u component of (a)–(c) velocity, (d)–(f) total (grid-resolved + SGS) TKE, and (g)–(i) temperature, downwind of the burn zone, at z/h = (left) 0.06, (center) 0.5, and (right) 1.5, for the P experiment series. The period ±20 min from ignition is displayed.

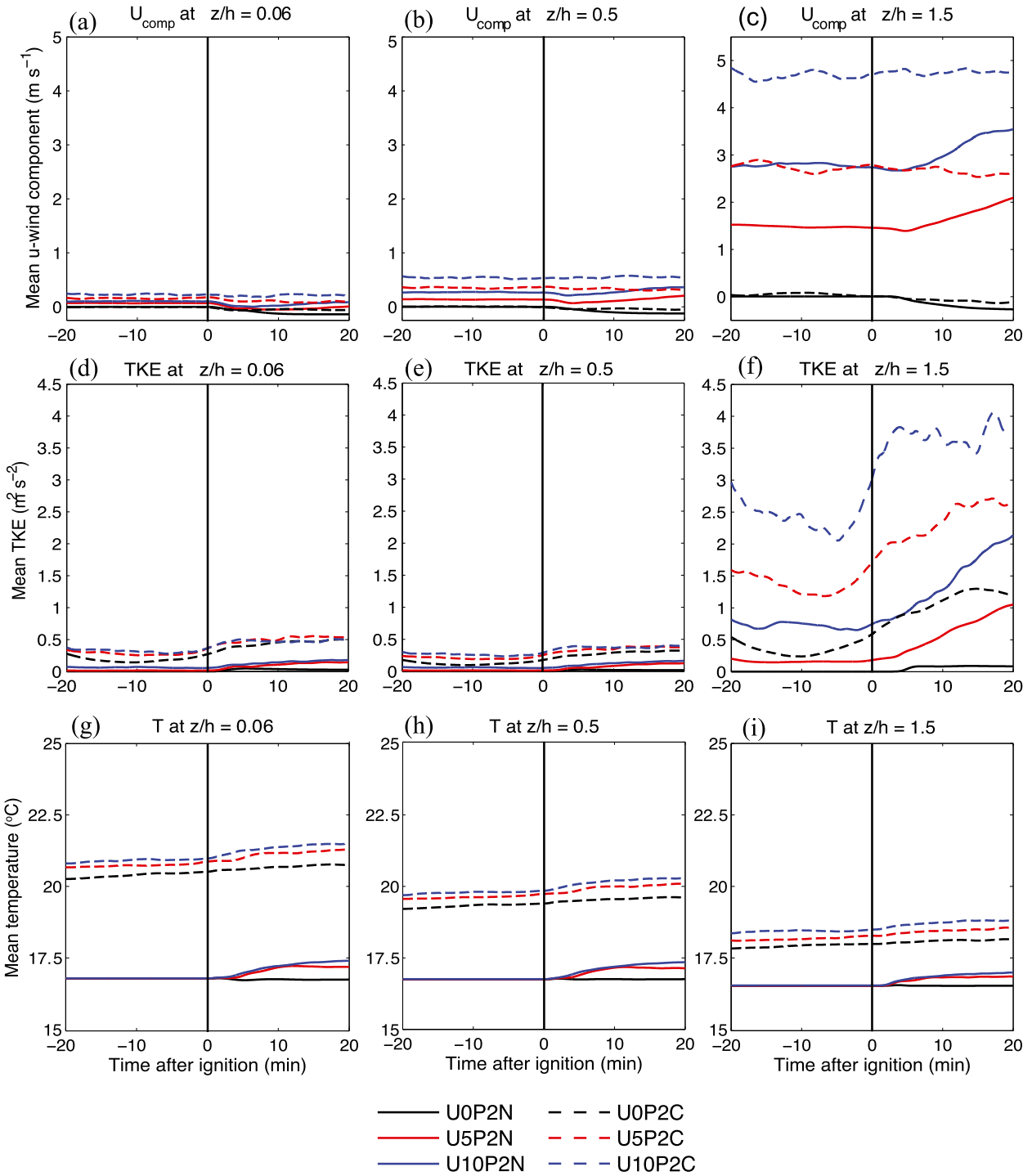

FIG. 3. As in Fig. 2, but for the *U* experiment series.

that is broadly similar to that of the P experiment series. Background wind serves to advect perturbations away from the fire, resulting in a more gradual decrease in variances downstream of the fire as background wind is increased (e.g., cf. U5P2N and U10P2N). In the cases with no background flow (U0P2N and U0P2C), the peak variances at all three levels remain near the fire.

To aid in visualization of the impact of the fire on vertical motion, horizontal cross sections of vertical

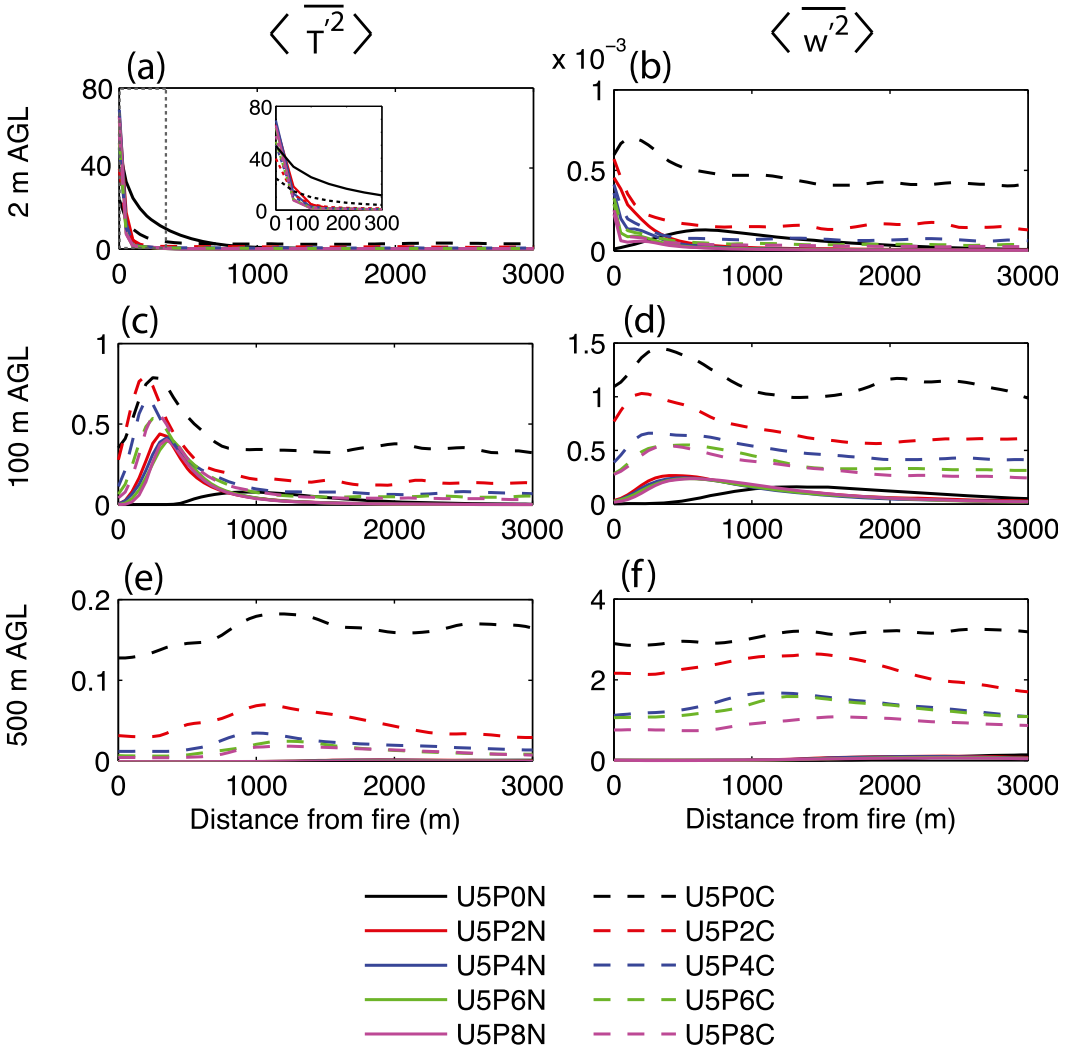

FIG. 4. Horizontal profiles of (a),(c),(e) temperature variance ($\langle\overline{T'^2}\rangle$; K^2) and (b),(d),(f) vertical velocity variance ($\langle\overline{w'^2}\rangle$; $m^2 s^{-2}$) downstream of the fire, for the *P* experiment series. Variances are averaged temporally over the fire period and spatially across the *y* domain. The inset panel in (a) depicts the area from 0 to 300 m downstream of the fire (see dashed line in main panel).

velocity at three levels within the roughness sublayer and PBL (27, 100, and 500 m AGL) are presented in Fig. 6 for cases U5P2N and U5P2C. A comparison of the left and right panels of Fig. 6 supports the earlier finding that the effect of the fire is most pronounced in the cases with a neutral background (e.g., U5P2N; left panels). In those cases, updrafts and downdrafts within the analysis region downstream of the fire (black rectangle) are stronger than their counterparts in the region upstream (i.e., to the left) of the fire. In cases with a convective background (e.g., U5P2C, right panels in Fig. 6), enhancement of vertical velocity by the fire is more difficult to discern, but the horizontal profiles of vertical velocity variance shown in Fig. 4 did indeed reveal a corridor of upward motion downstream of the fire emanating from the heat source. Note in Fig. 6 the orientation of convective elements with respect to the background (i.e., initial state) wind, especially in case U5P2N; the deviation of the rolls or streaks from a true west–east orientation is evidence of the Ekman spiral, wherein the wind increasingly deviates from geostrophic with decreasing altitude. In this study, the simulations are initialized with no v component of wind and the background westerly wind in ARPS is in geostrophic balance. Thus, when analyzing the u component of velocity (i.e., the fire-line-normal component) in this study, it must be understood that a small, but non-negligible, v component (i.e., fire-line-parallel component) of velocity, of positive sign, develops after initialization [$O(0.5\,m\,s^{-1})$].

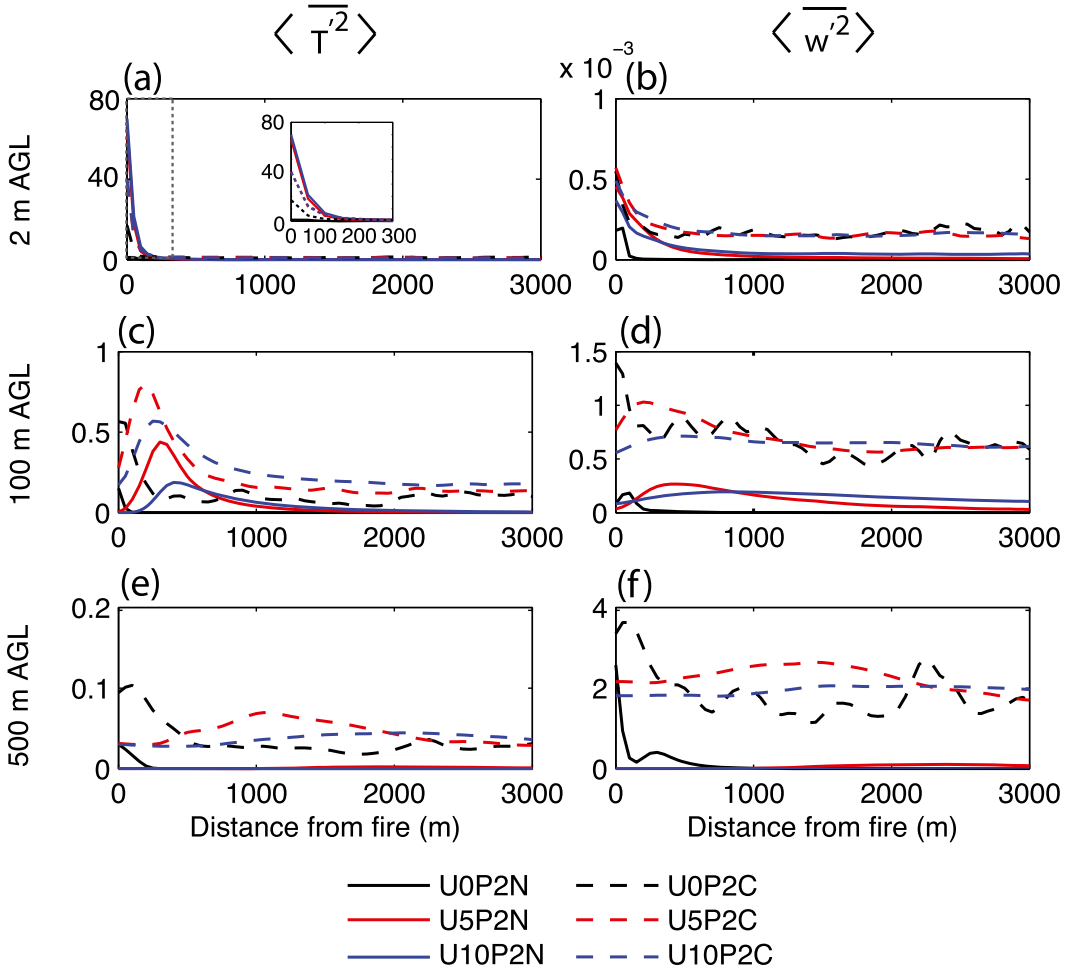

FIG. 5. As in Fig. 4, but for the *U* experiment series.

Up to this point, the sensitivity of mean and turbulent flow to a low-intensity fire has been examined for two experiment series: one wherein *P* is varied and the other in which *U* is varied. Since the influence of a forest canopy on atmospheric processes associated with low-intensity fires is a principal motivation for this study, the remainder of this paper will focus on the *P* experiment series.

b. The P experiment series: PBL scalar fluxes

In the preceding analysis, we examined the sensitivity of temperature and vertical velocity variances, computed at three levels in the PBL, to a low-intensity fire. We now consider the impact of a forest canopy on the vertical flux of scalar quantities associated with a low-intensity fire (e.g., heat and smoke) by examining downstream mean vertical turbulent heat flux throughout a 40-min period centered on ignition, in cases with neutral and convective background states (Figs. 7 and 8). Note that Figs. 7 and 8 consider the atmosphere from the surface to the top of the PBL.

Examining cases with a neutral background first (Fig. 7), we see that vertical heat flux is larger in case U5P2N than for U5P0N and weakens as canopy density is increased from $P = 2$ to $P = 8$. This finding is in general agreement with the temperature and vertical velocity variances in Fig. 4, wherein variances are larger in the U5P2N case than for the U5P0N case and gradually decrease as canopy density is increased (e.g., Figs. 4c,d). This decreasing trend in peak variances with increasing canopy density, while consistent, is small, however, and may in part be related to random error. Note also that the onset of fire-induced vertical heat flux in cases with a canopy is delayed by 2–3 min from the onset in the U5P0N case, although the onset timing shows no sensitivity to nonzero canopy density. The spatially averaged vertical heat flux is at most about $0.07\,\mathrm{K\,m\,s^{-1}}$ (about $75\,\mathrm{W\,m^{-2}}$) and is indicative of the atmosphere downstream of a low-intensity fire in an otherwise neutrally stratified environment. Thus, fire-induced convection (Fig. 6) supports the vertical flux of

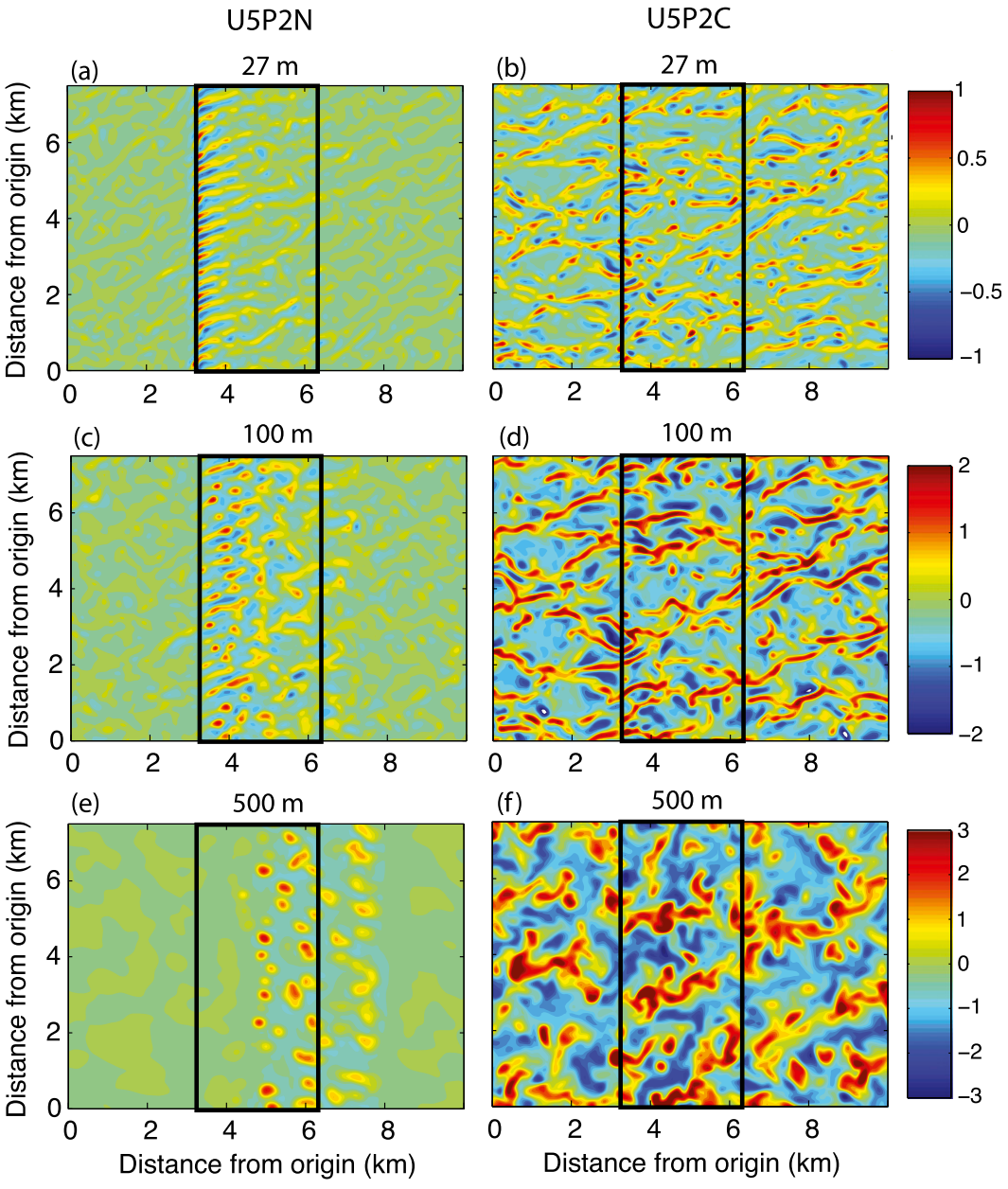

FIG. 6. Horizontal cross sections of instantaneous vertical velocity ($m\,s^{-1}$), 20 min after ignition, at (a),(b) 27, (c),(d) 100, and (e),(f) 500 m AGL for cases (left) U5P2N and (right) U5P2C. Note the change in contour limits between panels. The black rectangle denotes the averaging area used to compute spatially averaged quantities presented elsewhere in the paper (e.g., Fig. 2) and also indicates the *x*-axis bounds of Figs. 4 and 5.

heat through the PBL, with possible implications for the vertical transport of scalars (e.g., smoke).

The development of an upward heat flux within the PBL downstream of the fire suggests a reason for the increase in the above-canopy fire-line-normal wind component that occurs during the fire period in cases with a neutral background (Fig. 2c): in an otherwise weakly turbulent atmosphere, fire-induced convection promotes not only enhanced vertical mixing of heat but also enhanced downward mixing of higher-momentum air from aloft (not shown).

In the cases with a convective background (Fig. 8), the vertical heat flux is largest in case U5P0C, peaking at about $0.5\,K\,m\,s^{-1}$ (about $550\,W\,m^{-2}$), and steadily weakens as canopy density is increased. When the heat flux present during the prefire period is taken into account, we find that the response to the fire is actually strongest in the U5P2C case. This is best seen in Fig. 9,

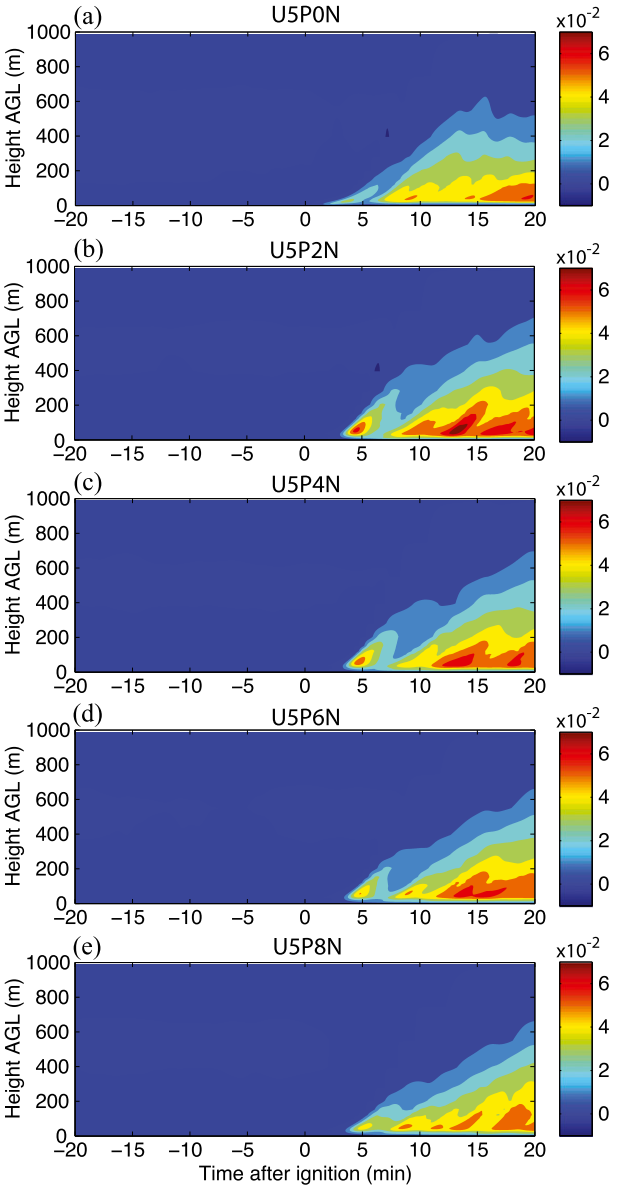

FIG. 7. Time–height cross sections of spatially averaged vertical turbulent heat flux (K m s^{-1}) in the PBL (0–1 km AGL) for the cases in the *P* experiment series with a neutral background. The period ±20 min from ignition is displayed.

wherein vertical heat flux integrated vertically and temporally (over the fire period) is presented in scatterplot form, with the prefire integrated value subtracted. With the prefire state thus removed, the same pattern is seen in cases with neutral and convective background states: the U5P2 cases exhibit stronger sensitivity of PBL-integrated vertical turbulent heat flux to the low-intensity fire than do the U5P0 cases, with sensitivity to the fire then decreasing as canopy density is further increased.

c. *The P experiment series: Grid-resolved TKE budget*

We now examine the physical processes underlying the evolution of TKE seen in Fig. 2, for cases U5P0C, U5P2C, and U5P8C. In the interest of eliminating higher-frequency, transient signals, we avoid time series of short-duration (e.g., 1 min) mean budget terms and instead choose to analyze vertical profiles averaged over 20-min periods. Before proceeding to the TKE budget, profiles of 20-min mean total and grid-resolved TKE are presented in Fig. 10 to provide context for the budget analysis that follows. In cases U5P2C and U5P8C, the mean TKE profile exhibits a ''classical'' canopy shape with relatively small TKE inside the canopy and an asymptotic increase in TKE above the canopy, consistent with field-experiment, theoretical, and numerical-modeling results (e.g., Dwyer et al. 1997; Finnigan 2000; Dupont and Brunet 2008). The maximum proportion of total TKE that is parameterized ($\mathrm{TKE_{SGS}/TKE_{Total}}$) varies considerably among the three experiments, from no more than 15% in U5P0C to ~25% in U5P2C and ~50% in U5P8C. Note, however, that the highest ratios are restricted to levels inside the canopy where total TKE is small (0.25 m^2 s^{-2} or less). In each case, the amount of total TKE is larger during the fire period while the proportion of SGS TKE is actually smaller. Recall from section 3a that for cases with a convective background the larger quantity of mean TKE during the fire period is related in part to variability in the prefire TKE. Thus, in analyzing the TKE budget, it must be understood that differences in forcing terms between the two time periods do not result from application of the fire alone.

With the profiles of total and grid-resolved TKE in mind, we proceed to the budget of grid-resolved TKE. Using Einstein notation, the budget of mean grid-resolved TKE $\overline{E}$ may be expressed as

$$\begin{aligned}\frac{\partial \overline{E}}{\partial t} &= \underbrace{-\overline{u_j}\frac{\partial \overline{E}}{\partial x_j}}_{\text{(TND)}} \underbrace{-\overline{u_i'u_j'}\frac{\partial \overline{u_i}}{\partial x_j}}_{\text{(ADV)}} \underbrace{+\delta_{i3}\frac{g}{\theta_o}\overline{u_i'\theta'}}_{\text{(SHR)}} \underbrace{-\frac{\partial(\overline{u_j'E})}{\partial x_j}}_{\text{(BUO)}} \\ &\quad \underbrace{-\frac{1}{\rho}\frac{\partial(\overline{u_i'p'})}{\partial x_i}}_{\text{(TTR)}} \underbrace{+\overline{u_i'F_i'}}_{\text{(PTR)}} \underbrace{-\frac{2}{3}\frac{\partial(u_i'e')}{\partial x_i}}_{\text{(CDR)}} \underbrace{+\frac{\partial(u_i'\tau_{ij}')}{\partial x_j}}_{\text{(TTS)}} \underbrace{+\overline{\tau_{ij}'\frac{\partial u_i'}{\partial x_j}}}_{\text{(DIS)}}, \end{aligned} \tag{1}$$

where e is the SGS TKE component, $\tau_{ij} = -K_M(\partial u_i/\partial x_j + \partial u_j/\partial x_i)$ is the Reynolds stress tensor, and $F_i = -C_d\alpha\rho A_p(z)Vu_i$ is the canopy drag force in the x_i direction. In Eq. (1), **u** is wind velocity, θ is potential

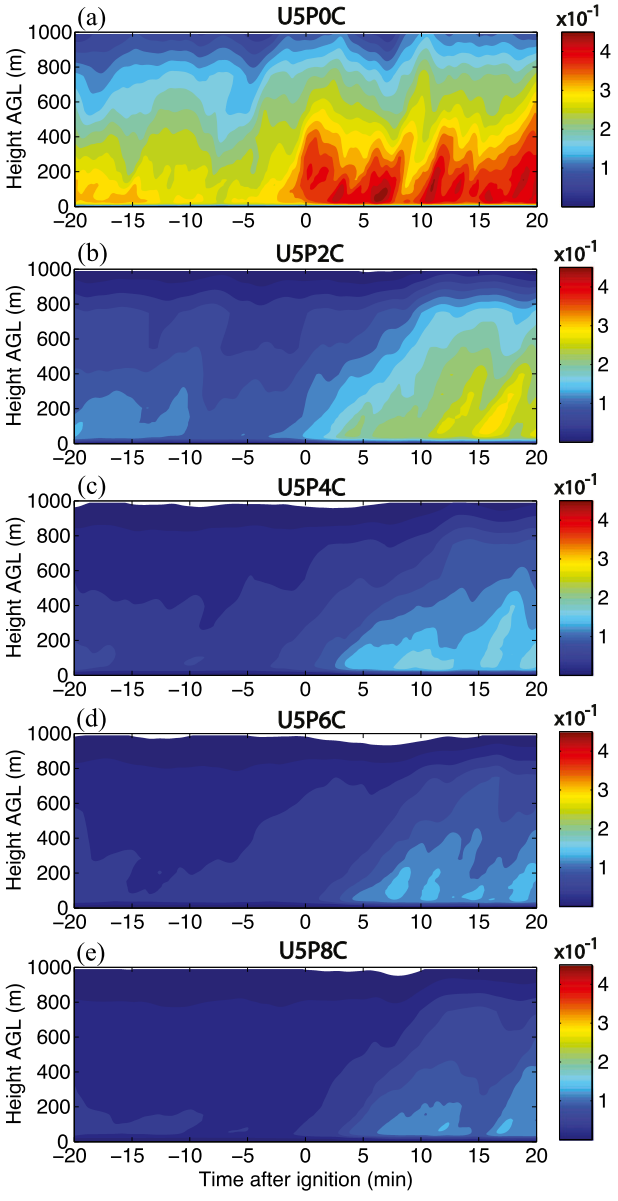

FIG. 8. As in Fig. 7, but for cases with a convective background. Note the difference in the color-bar scaling between Figs. 7 and 8.

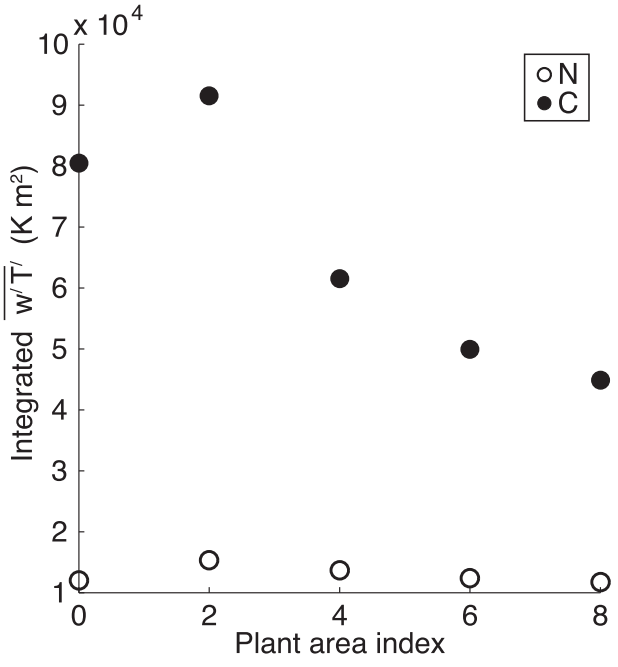

FIG. 9. Scatterplot of vertically and temporally integrated mean vertical turbulent heat flux (K m^2), computed as the integral over the 20-min period following ignition, minus the integral over the 20-min period prior to ignition. Labels N and C refer to cases with neutral and convective background states, respectively.

temperature, p is pressure, and ρ is density. Furthermore, K_M is eddy viscosity, C_d is a canopy drag coefficient [set equal to 0.2 following Kiefer et al. (2013)], α is fraction of ground covered by trees (arbitrarily set to 0.75 in this study), and V is mean wind speed. A line above a term or variable denotes time averaging, whereas a prime symbol denotes a perturbation from a time average.

The terms in Eq. (1) are, from left to right, tendency (TND), advection (ADV), shear production (SHR), buoyant production/destruction (BUO), turbulent transport by resolved eddies (TTR), pressure transport (PTR), rate of work done by velocity perturbations against canopy drag (CDR), turbulent transport by SGS eddies (TTS), and free-air dissipation of grid-resolved TKE (DIS). For convenience, we sum TTR and TTS and present the total turbulent transport (TTT). Because of uncertainty in computing static perturbation pressure p', we do not compute PTR but instead include it in the residual (RES), the latter computed by subtracting the sum of the computed terms on the right-hand side from TND. All terms are averaged in space downstream of the fire line (as described in section 2c).

Examining the prefire period first (Fig. 11, left panels), we see that BUO is the dominant TKE production term in the U5P0C case, with SHR dominant in cases U5P2C and U5P8C. In the light-wind environment ($U = 5\,\mathrm{m\,s^{-1}}$), SHR only plays a primary role in turbulence evolution when a canopy is present. TTT and PTR (as interpreted from RES) are present in all three cases but transport turbulence vertically in different ways with and without a canopy. In the U5P0C case, TTT is of negative sign throughout the profile, with the exception of the surface, and PTR opposes (reinforces) TTT below (above) ~10 m AGL. In the U5P2C and U5P8C cases, TTT is of positive (negative) sign below (above) the canopy top, indicating downward transport of turbulence into the canopy, with PTR being the only source term deep within the canopy. The DIS term is larger in the U5P2C and U5P8C cases than

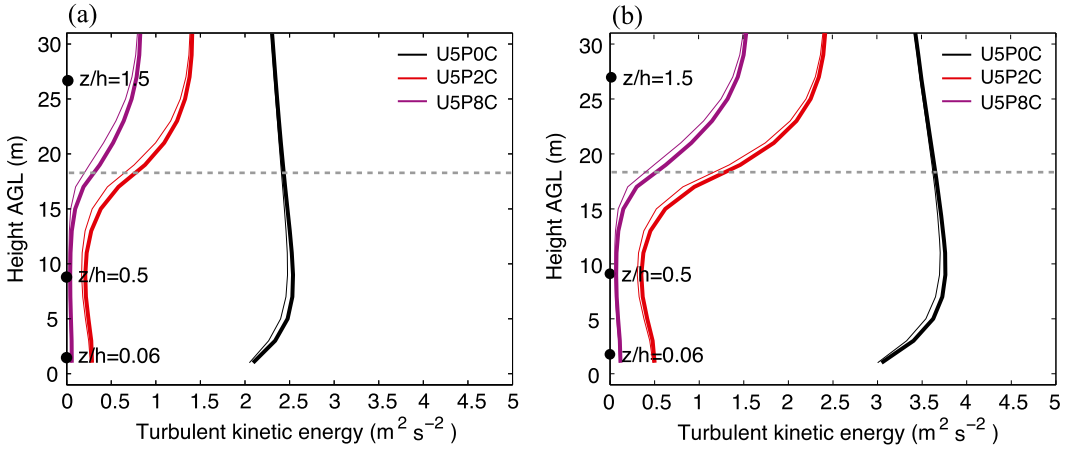

FIG. 10. Vertical profiles of spatially averaged total TKE ($m^2 s^{-2}$; thick lines) and grid-resolved TKE (thin lines), averaged temporally over the 20-min periods (a) before ignition and (b) following ignition, for cases U5P0C, U5P2C, and U5P8C. Filled circles denote the levels examined in Fig. 2. The top of the canopy is indicated with a dashed gray line.

in the U5P0C case, with the CDR term being larger in magnitude and maximized at a slightly lower height in the upper canopy than DIS. Deep within the canopy, the only active terms are CDR and PTR. The profiles of grid-resolved TKE budget terms in the U5P2C and U5P8C cases are in broad agreement with grid-resolved TKE budgets computed from field-experiment data and LES-model output (e.g., Meyers and Baldocchi 1991; Dwyer et al. 1997).

In comparing the fire and prefire periods, we see that the increase in mean TKE (Fig. 10b) is a consequence of an increase in the strength of the buoyancy and shear production terms [mainly buoyancy in case U5P0C (Fig. 11b) and both buoyancy and shear in cases U5P2C and U5P8C (Figs. 11d,f)]. Note that the increase in shear production in the cases with a convective background is mainly the result of an increase in the vertical shear of the fire-line-parallel wind component that begins prior to ignition (not shown), because the vertical shear of the fire-line-normal component is largely unchanged during the 40-min analysis window (see time series of the fire-line-normal wind component at $z/h = 0.5$ and $z/h = 1.5$; Figs. 2b,c). In cases with a neutral background, however, variation of the fire-line-parallel component is small (not shown), and the increase in shear production is mainly attributable to an increase in the vertical shear of the fire-line-normal wind component following ignition (Figs. 2b,c). The increase in the magnitude of the production terms is accompanied by a commensurate increase in the magnitude of the dissipation (CDR and DIS) terms. Changes to the transport terms are less consistent between cases, with TTT modestly increasing in magnitude above 20 m AGL in cases U5P0C and U5P2C and PTR generally increasing in magnitude both inside and above the canopy in cases U5P2C and U5P8C.

4. Summary and conclusions

In this study, ARPS-CANOPY has been utilized to examine the sensitivity of mean and turbulent flow downstream of a low-intensity surface fire to environmental factors including canopy density, background wind speed, and background instability. Analysis of the grid-resolved TKE budget has also been performed to examine production, transport, and dissipation of turbulence before and during a low-intensity fire, in both sparse and dense canopies. In all experiments, the model was run for 3 h to produce a horizontally homogeneous and quasi-stationary PBL, after which time a 5 kW m^{-2} surface heat flux was applied along a line of grid cells oriented normal to the background wind. Because the stated focus of the study is the area downstream of the fire and not the atmosphere directly above it, analysis was restricted to a zone beginning immediately downstream of the fire line and extending 3 km farther downstream.

Analysis of all 14 experiments showed that, in general, roughness sublayer turbulence both prior to and during the low-intensity fire was damped in the presence of a canopy. In cases with a neutral background, the increase in TKE during the fire period was unambiguous. In cases with a convective background, however, variability of TKE in the prefire environment was comparable in magnitude to the variability exhibited during the fire period. An analysis of the grid-resolved TKE budget in the roughness sublayer revealed that the larger TKE present during the fire period was associated with an increase in buoyancy production in the case with no canopy and an increase in both buoyancy and shear production in the cases with a canopy.

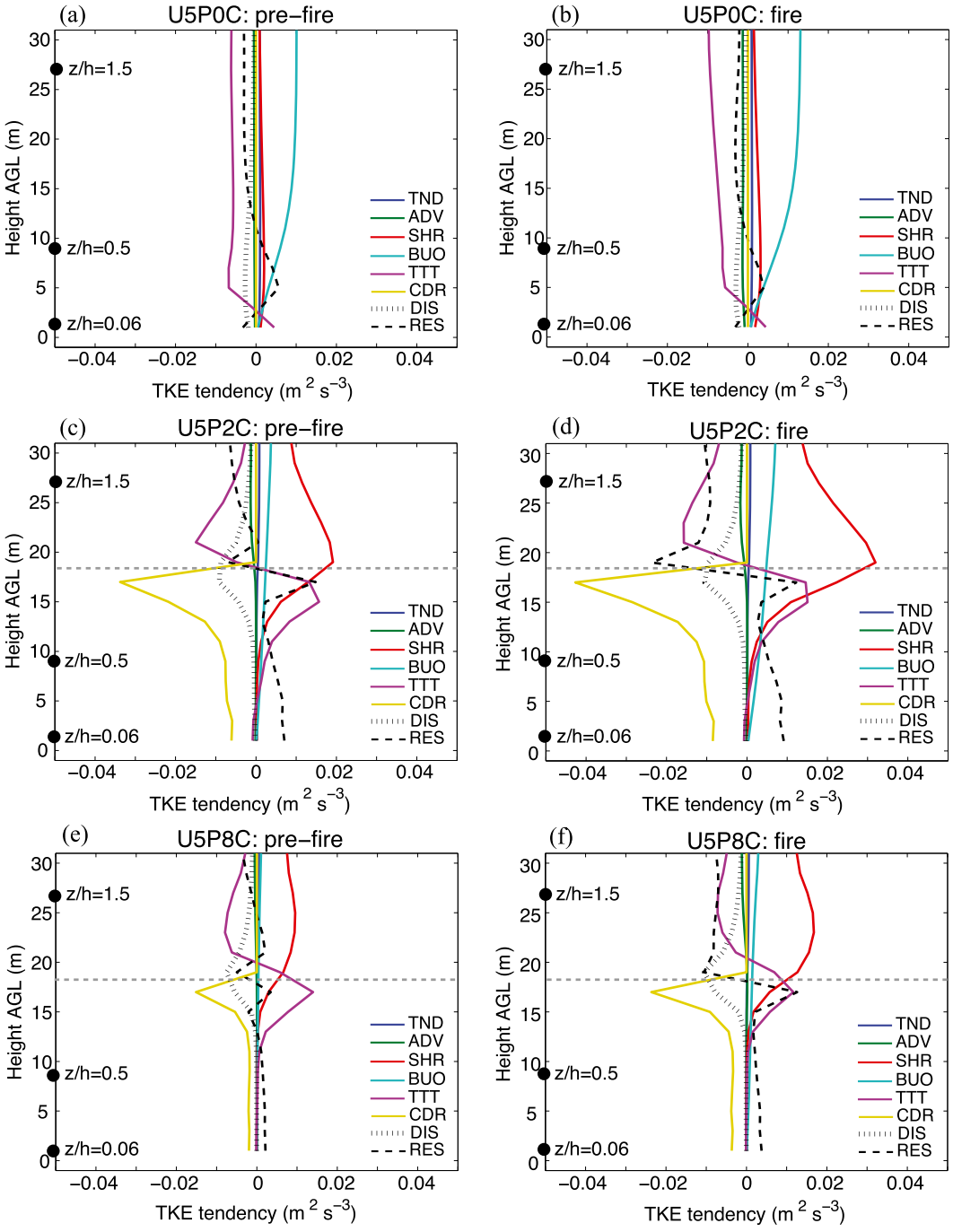

FIG. 11. Vertical profiles of spatially averaged grid-resolved TKE budget forcing terms from cases (a),(b) U5P0C, (c),(d) U5P2C, and (e),(f) U5P8C, averaged temporally over the 20-min periods (left) prior to and (right) following ignition. Filled circles denote the levels examined in Fig. 2. The top of the canopy is indicated with a dashed gray line in (c)–(f).

Both prior to and during the fire period, the fire-line-normal component of wind in the roughness sublayer was shown to be weaker with a sparse canopy than with no vegetation, although it was mostly insensitive to further increases in canopy density. With a convective background, the fire-line-normal wind component was found to vary little between the prefire and fire periods; with a neutral background, however, a steady increase in the fire-line-normal component above the canopy (or ground surface in the case with no canopy) occurred as

a result of an increase in turbulent mixing of higher momentum from aloft in an otherwise weakly turbulent neutrally stratified atmosphere. Sensitivity of maximum updraft strength to the fire was shown to be largely independent of the density of canopy vegetation, but the impact of the fire on PBL-integrated vertical turbulent heat flux was strongest with a sparse canopy and gradually weakened with increasing canopy density.

From the outcome of the sensitivity experiments, we recommend caution when applying ARPS simulation results to predictions of smoke transport and dispersion. The impact of the parameterized forest canopy on simulated mean and turbulent flow downstream of the fire, as well as the vertical flux of scalars (e.g., smoke) through the roughness sublayer and PBL, suggests that transport and dispersion of smoke are likely to be sensitive to the way in which the canopy effects on the atmosphere (e.g., drag) are accounted for in the model (e.g., roughness length or canopy submodel). Furthermore, we recommend caution when applying results of neutral-stratification simulations to daytime unstable conditions, because the impact of the low-intensity fire on mean and turbulent flow may be overstated.

This study has provided insight into atmospheric flow sensitivities that have the potential to impact predictions of smoke dispersion from low-intensity fires. A logical next step from the current study is to perform simulations of actual smoke transport and dispersion, with the meteorological fields from the ARPS-CANOPY simulations as driving inputs. To accomplish this goal, we will utilize the Pacific Northwest National Laboratory Integrated Lagrangian Transport (PILT) model [a recently revised version of the Flexible Particle Dispersion Model (FLEXPART; Stohl et al. 2005; Fast and Easter 2006)]. Sensitivity of smoke-plume characteristics to canopy density, wind speed, and background stability will be examined in future work. Furthermore, in this study we have only considered a limited subset of potentially relevant parameters. Future work will also include an examination of the sensitivity of mean and turbulent flow downstream of a fire to additional parameters including canopy shape, fire intensity, ambient vertical wind shear, and stable stratification.

Acknowledgments. Support for this research was provided by the U.S. Joint Fire Science Program (Project 09-1-04-1) and the USDA Forest Service (Research Joint Venture Agreement 09-JV-11242306-089). We thank Jovanka Nikolic, Lisi Pei, and two anonymous reviewers for reviewing the manuscript and providing helpful comments.

REFERENCES

Chou, M.-D., 1990: Parameterization for the absorption of solar radiation by O_2 and CO_2 with application to climate studies. *J. Climate,* **3,** 209–217, doi:10.1175/1520-0442(1990)003<0209:PFTAOS>2.0.CO;2.

——, 1992: A solar radiation model for climate studies. *J. Atmos. Sci.,* **49,** 762–772, doi:10.1175/1520-0469(1992)049<0762:ASRMFU>2.0.CO;2.

——, and M. J. Suarez, 1994: An efficient thermal infrared radiation parameterization for use in general circulation models. NASA Tech. Memo. 104606, 85 pp. [Available from NASA Center for Aerospace Information, 800 Elkridge Landing Rd., Linthicum Heights, MD 21090-2934.]

Clements, C. B., and Coauthors, 2007: Observing the dynamics of wildland grass fires: FireFlux—A field validation experiment. *Bull. Amer. Meteor. Soc.,* **88,** 1369–1382, doi:10.1175/BAMS-88-9-1369.

Cunningham, P., S. L. Goodrick, M. Y. Hussaini, and R. R. Linn, 2005: Coherent vortical structures in numerical simulations of buoyant plumes from wildland fires. *Int. J. Wildland Fire,* **14,** 61–75, doi:10.1071/WF04044.

Dupont, S., and Y. Brunet, 2008: Influence of foliar density profile on canopy flow: A large-eddy simulation study. *Agric. For. Meteor.,* **148,** 976–990, doi:10.1016/j.agrformet.2008.01.014.

——, and ——, 2009: Coherent structures in canopy edge flow: A large-eddy simulation study. *J. Fluid Mech.,* **630,** 93–128, doi:10.1017/S0022112009006739.

Dwyer, M. J., E. G. Patton, and R. H. Shaw, 1997: Turbulent kinetic energy budgets from a large eddy simulation of airflow above and within a forest canopy. *Bound.-Layer Meteor.,* **84,** 23–43, doi:10.1023/A:1000301303543.

Fast, J. D., and R. C. Easter, 2006: A Lagrangian particle dispersion model compatible with WRF. *Proc. Seventh Annual WRF User's Workshop,* Boulder, CO, NCAR, 5 pp. [Available online at http://www2.mmm.ucar.edu/wrf/users/workshops/WS2006/abstracts/PSession06/P6_02_Fast.pdf.]

Finnigan, J. J., 2000: Turbulence in plant canopies. *Annu. Rev. Fluid Mech.,* **32,** 519–571, doi:10.1146/annurev.fluid.32.1.519.

Heilman, W. E., and J. D. Fast, 1992: Simulations of horizontal roll vortex development above lines of extreme surface heating. *Int. J. Wildland Fire,* **2,** 55–68, doi:10.1071/WF9920055.

——, and Coauthors, 2013: Development of modeling tools for predicting smoke dispersion from low-intensity fires. Joint Fire Science Plan Study Final Rep. 09-1-04-1, 64 pp.

Hiers, J. K., R. Ottmar, B. W. Butler, C. Clements, R. Vihnanek, M. B. Dickinson, and J. O'Brien, 2009: An overview of the Prescribed Fire Combustion and Atmospheric Dynamics Research Experiment (Rx-CADRE). *Proc. Fourth Int. Fire Ecology and Management Congress: Fire as a Global Process,* Savannah, GA, Association for Fire Ecology.

Kanda, M., and M. Hino, 1994: Organized structures in developing turbulent flow within and above a plant canopy, using a large eddy simulation. *Bound.-Layer Meteor.,* **68,** 237–257, doi:10.1007/BF00705599.

Kiefer, M. T., and S. Zhong, 2013: The effect of sidewall forest canopies on the formation of cold-air pools: A numerical study. *J. Geophys. Res. Atmos.,* **118,** 5965–5978, doi:10.1002/jgrd.50509.

——, Y.-L. Lin, and J. J. Charney, 2008: A study of two-dimensional dry convective plume modes with variable critical level height. *J. Atmos. Sci.,* **65,** 448–469, doi:10.1175/2007JAS2301.1.

——, M. D. Parker, and J. J. Charney, 2009: Regimes of dry convection above wildfires: Idealized numerical simulations and dimensional analysis. *J. Atmos. Sci.,* **66,** 806–836, doi:10.1175/2008JAS2896.1.

——, S. Zhong, W. E. Heilman, J. J. Charney, and X. Bian, 2013: Evaluation of an ARPS-based canopy flow modeling system for use in future operational smoke prediction efforts. *J. Geophys. Res. Atmos.,* **118,** 6175–6188, doi:10.1002/jgrd.50491.

——, and Coauthors, 2014: Multiscale simulation of a prescribed fire event in the New Jersey Pine Barrens using ARPS-CANOPY. *J. Appl. Meteor. Climatol.,* **53,** 793–812, doi:10.1175/JAMC-D-13-0131.1.

Linn, R. R., and P. Cunningham, 2005: Numerical simulations of grass fires using a coupled atmosphere–fire model: Basic fire behavior and dependence on wind speed. *J. Geophys. Res.,* **110,** D13107, doi:10.1029/2004JD005597.

Melvin, M. A., 2012: 2012 National prescribed fire use survey report. Coalition of Prescribed Fire Councils Inc. Tech. Rep. 01-12, 24 pp. [Available online at http://www.stateforesters.org/sites/default/files/publication-documents/2012_National_Prescribed_Fire_Survey.pdf.]

Meyers, T. P., and D. D. Baldocchi, 1991: The budgets of turbulent kinetic energy and Reynolds stress within and above a deciduous forest. *Agric. For. Meteor.,* **53,** 207–222, doi:10.1016/0168-1923(91)90058-X.

Michioka, T., and F. K. Chow, 2008: High-resolution large-eddy simulations of scalar transport in atmospheric boundary layer flow over complex terrain. *J. Appl. Meteor. Climatol.,* **47,** 3150–3169, doi:10.1175/2008JAMC1941.1.

Parker, M. D., and R. H. Johnson, 2004: Structures and dynamics of quasi–2D mesoscale convective systems. *J. Atmos. Sci.,* **61,** 545–567, doi:10.1175/1520-0469(2004)061<0545:SADOQM>2.0.CO;2.

Pimont, F., J. L. Dupuy, R. R. Linn, and S. Dupont, 2009: Validation of FIRETEC wind-flows over a canopy and a fuel-break. *Int. J. Wildland Fire,* **18,** 775–790, doi:10.1071/WF07130.

——, ——, ——, and ——, 2011: Impacts of tree canopy structure on wind flows and fire propagation simulated with FIRETEC. *Ann. For. Sci.,* **68,** 523–530, doi:10.1007/s13595-011-0061-7.

Skamarock, W. C., J. B. Klemp, and J. Dudhia, D. O. Gill, D. M. Barker, W. Wang, and J. G. Powers, 2005: A description of the Advanced Regional WRF version 2. NCAR Tech. Note NCAR/TN-468+STR, 88 pp. [Available online at http://www2.mmm.ucar.edu/wrf/users/docs/arw_v2.pdf.]

Stohl, A., C. Forster, A. Frank, P. Seibert, and G. Wotawa, 2005: Technical note: The Lagrangian particle dispersion model FLEXPART version 6.2. *Atmos. Chem. Phys.,* **5,** 2461–2474, doi:10.5194/acp-5-2461-2005.

Sun, H., T. L. Clark, R. B. Stull, and T. A. Black, 2006: Two-dimensional simulation of airflow and carbon dioxide transport over a forested mountain. Part I: Interactions between thermally-forced circulations. *Agric. For. Meteor.,* **140,** 338–351, doi:10.1016/j.agrformet.2006.03.023.

Sun, R., M. A. Jenkins, S. K. Krueger, W. Mell, and J. J. Charney, 2006: An evaluation of fire-plume properties simulated with the Fire Dynamics Simulator (FDS) and the Clark coupled wildfire model. *Can. J. For. Res.,* **36,** 2894–2908, doi:10.1139/x06-138.

——, S. K. Krueger, M. A. Jenkins, M. A. Zulauf, and J. J. Charney, 2009: The importance of fire-atmosphere coupling and boundary layer turbulence to wildfire spread. *Int. J. Wildland Fire,* **18,** 50–60, doi:10.1071/WF07072.

Xue, M., K. K. Droegemeier, and V. Wong, 2000: The Advanced Regional Prediction System (ARPS)—A multi-scale nonhydrostatic atmosphere simulation and prediction model. Part I: Model dynamics and verification. *Meteor. Atmos. Phys.,* **75,** 161–193, doi:10.1007/s007030070003.

——, ——, ——, A. Shapiro, K. Brewster, F. Carr, D. Weber, Y. Liu, and D. Wang, 2001: The Advanced Regional Prediction System (ARPS)—A multi-scale nonhydrostatic atmosphere simulation and prediction tool. Part II: Model physics and applications. *Meteor. Atmos. Phys.,* **76,** 143–165, doi:10.1007/s007030170027.

——, D. Wang, J. Gao, K. Brewster, and K. K. Droegemeier, 2003: The Advanced Regional Prediction System (ARPS), storm-scale numerical weather prediction and data assimilation. *Meteor. Atmos. Phys.,* **82,** 139–170. [Available online at http://kkd.ou.edu/ARPSPaperIII.pdf.]